Chemical Physics Letters 504 (2011) 180–184

Contents lists available at ScienceDirect

Chemical Physics Letters

journal homepage: www.elsevier.com/locate/cplett

Controlling super-cooling of encapsulated phase change nanoparticles for enhanced heat transfer

Yan Hong [a,b,1], Wei Wu [b,1], Jianjun Hu [c], Minghui Zhang [d], Andrey A. Voevodin [c], Louis Chow [b], Ming Su [a,b,*]

[a] NanoScience Technology Center, University of Central Florida, Orlando, Florida 32826, USA
[b] Department of Mechanical, Materials and Aerospace Engineering, University of Central Florida, Orlando, FL 32826, USA
[c] Materials and Manufacturing Directorate, Air Force Research Laboratory, Wright-Patterson Air Force Base, Dayton, OH 45433, USA
[d] Institute of New Catalytic Materials Science, College of Chemistry, Nankai University, Tianjin, 300071, PR China

ARTICLE INFO

Article history:
Received 9 December 2010
In final form 23 January 2011
Available online 26 January 2011

ABSTRACT

Adding phase change nanoparticles into fluid enhances heat capacity, but supercooling of nanoparticles requires fluid working with large temperature difference, which limits heat transfer benefit. This Letter describes a method to reduce supercooling by encapsulating indium nanoparticles in non-melting shells of semi-crystalline silica derived from sodium silicate. Not only can the rough surface and matching structure of shells prevent molten cores from leakage or agglomeration, they allow heterogeneous nucleation during, solidification of nanoparticles and reduce supercooling up to 30 °C. The operating parameter including overheating, heating and cooling rates can be adjusted to reduce supercooling by 7 °C for silica shells derived from tetraethylorthosilicate.

Published by Elsevier B.V.

Phase change nanoparticles (nano-PCM) has been used as heat transfer additives in single phase liquid to enhance heat capacity for cooling applications. The dielectric property of liquid is preserved by encapsulating nanoparticles with highly dielectric and high-melting point silica derived from tetraethylorthosilicate (TEOS) [1]. One challenge is that the liquid to solid phase change occurs mainly through homogeneous nucleation with large degree of super-cooling [2], which leads to limited enhancement of heat transfer performance, because the effective specific heat of fluid containing nano-PCMs is defined as $C_{eff} = C_0 + H/\Delta T$, where H is the latent heat of fusion of nanoparticles, C_0 is the heat capacity of base fluid, and ΔT is degree of super-cooling as shown in Figure 1. Instead of taking temperature difference between two maximums, ΔT is defined as the difference between the highest temperature in melting peak and the lowest temperature in solidifying peak. The super-cooling of microsized particles of phase change materials can be reduced by adding nucleating agent to reduce nucleation barrier [3–8] or controlling working conditions such as degree of over-heating and cooling rates [9,10]. However there is no effective way to reduce super-cooling of metallic nanoparticles, which cannot be doped readily with non-molten impurities due to small size and lack of material with matching structure. Although previous studies have shown interface may play an important role in super-cooling of nanoparticles embedded in solid matrix [11], it is a challenge to control the interface property of shells to reduce supercooling of discrete phase change nanoparticles, which will be suspended in liquid for heat transfer. This Letter reports a method to reduce supercooling of molten indium nanoparticles by encapsulating in high-melting point semi-crystalline silica, which facilitates heterogeneous nucleation and prevents molten cores from leakage and agglomeration.

Indium powders are directly boiled in poly-α-olefin (PAO) to make indium nanoparticles at 200 °C. After removing nanoparticles from PAO by centrifuging and re-dispersing in ethanol or water, sol–gel method is used to encapsulate nanoparticles in silica shells. Two types of silica precursors have been used for encapsulation. (1) Tetraethylorthosilicate (TEOS) is added in an ethanol suspension of indium nanoparticles, followed by dropwise addition of ammonium hydroxide at 60 °C under sonication. After reacting for 90 min, nanoparticles with silica shells are washed by ethanol and dried at 110 °C. (2) A diluted solution of sodium silicate in water is added into nanoparticle suspension under sonication, followed by dropwise addition of hydrochloric acid until the pH reaches 9 at 60 °C. After reacting for 60 min, encapsulated nanoparticles are centrifuged and washed by ethanol and dried at 110 °C. Figure 2A is a transmission electron microscope (TEM) image of indium nanoparticles encapsulated in TEOS-derived silica, where core diameters and shell thickness are 200 and 100 nm, respectively. Figure 2B is a TEM image of indium nanoparticles encapsulated in silica derived from sodium silicate (water glass), where core diameter and shell thickness are 200 and 50 nm, respectively. The quantitative roughnesses of silica films derived from TEOS and sodium silicate are derived from atomic force

* Corresponding author. at: University of Central Florida, Orlando, Florida 32826, USA
E-mail address: mingsu@mail.ucf.edu (M. Su).
[1] Both of them contribute equally to this work.

0009-2614/$ - see front matter Published by Elsevier B.V.
doi:10.1016/j.cplett.2011.01.061

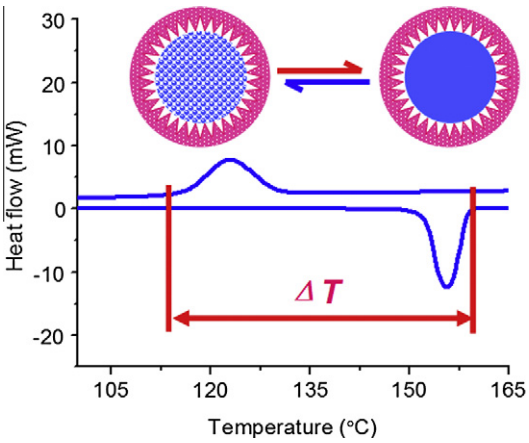

Figure 1. Supercooling of encapsulated phase change (indium) nanoparticles.

microscopy (AFM). Figure 2A and 2B insets show AFM images of silica films, where RMS (root-mean-square) roughness of silica from sodium silicate (127.4 nm) is larger than that from TEOS (22.4 nm), which is also confirmed by the facts that porosity of pure silica powders from sodium silicate (350 cm^3/g, black square) is larger that of silica from TEOS (~35 cm^3/g, red dot) (Figure 2C inset); and indium nanoparticles encapsulated inside two types of silica (Figure 2C). X-ray diffraction (XRD) analysis has been used to determine structures of silica formed around indium nanoparticles. Figure 2D shows that silica derived from TEOS is amorphous with a hump at 15–30°; and silica derived from sodium silicate has semi-crystallized structure with strong and sharp diffraction peaks at 32.3, 40.9 and 44.5°. The crystal structure of silica from sodium silicate is determined to be cristobalite by comparing its diffraction pattern with those in JADE database. Although its tetrahedral structure is stable at high temperature, a tetragonal form of cristobalite (Pearson symbol tP12) is stable at ambient pressure at temperature below 250 °C. The existence of cristobalite phase at lower temperature is due to large activation energy related to phase transition from cristobalite to quartz, which needs to break and reform silica framework.

Differential scanning calorimetry (Perkin Elmer DSC7) is used to measure thermal physical properties of uncoated nanoparticles, nanoparticles coated in TEOS-derived silica, and nanoparticles coated in sodium silicate derived silica. Figure 3A shows DSC curves collected at ramp rate of 10 °C/min, where all indium materials melt at 155.2 °C, but freeze are different temperature: raw powders and nanoparticles in TEOS-derived silica freeze at 131.2 and 123.6 °C, respectively; nanoparticles coated in sodium silicate derived silica freeze at 148.6 °C, and bulk indium freezes at 150.4 °C. The solidification of molten indium can occur through either homogeneous or heterogeneous nucleation depending whether there are nucleating sites. In the absence of gravity contribution, the critical Gibbs free energy of nucleation of molten indium ($\Delta G*$) is given by

$$\Delta G^* = \frac{16\pi\gamma_{SL}^3 T_m^2}{3\Delta H^2 \Delta T^2} \quad (1)$$

Where $f(\theta) = \frac{1}{4}(2+\cos\theta)(1-\cos\theta)^2$, $\cos\theta = \frac{\gamma_{SL}-\gamma_{SM}}{\gamma_{SL}}$ and θ is the contact angle of molten indium on solid, ΔH is the latent heat of fusion of indium, γ_{SL} is the interfacial energy between solid and liquid interface. Assuming that interface between indium and silica is planar, the interfacial energy (γ_{SM}) can be derived from

$$\gamma_{SM} = \gamma_S + \gamma_M - 2\sqrt{\gamma_S\gamma_M} = \left(\sqrt{\gamma_S} - \sqrt{\gamma_M}\right)^2 \quad (2)$$

where γ_S and γ_M are surface energies of molten indium, and silica, respectively. Table 1 lists interfacial energies between molten indium and silica of different crystal face, where values of indium-

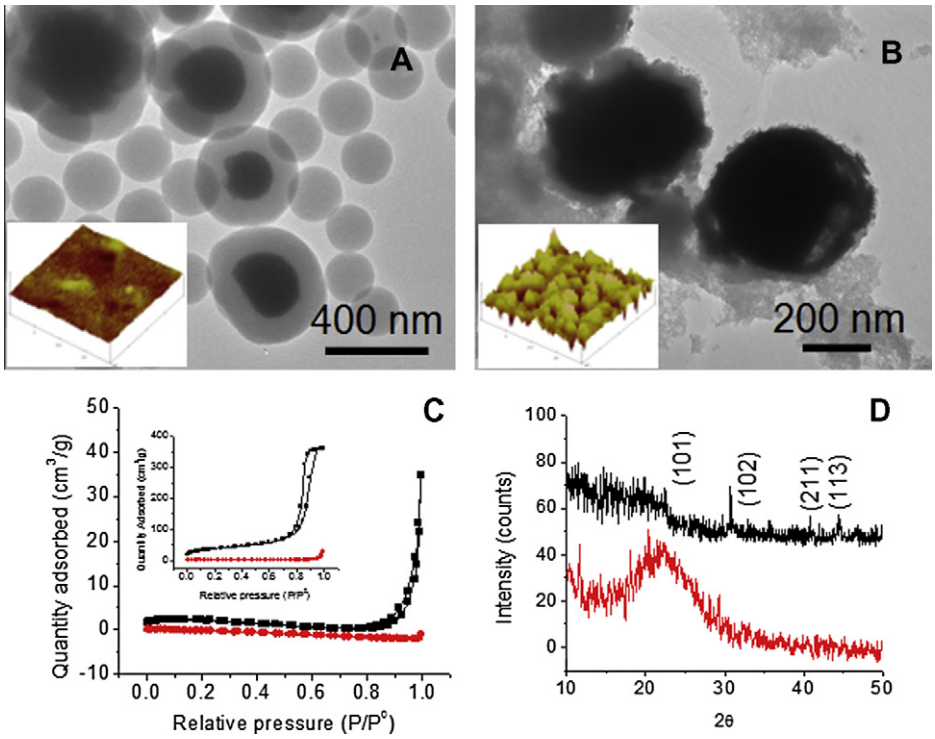

Figure 2. TEM images of indium nanoparticles encapsulated in silica derived from TEOS (A), and sodium silicate (B); AFM images (40 × 40 μm scanning range) of silica films obtained from TEOS (A inset) and sodium silicate (B inset); nitrogen adsorptions of indium nanoparticles coated in TEOS-derived silica (red dot) and sodium silicate derived silica (black square) (C); and according adsorptions of pure silica powders derived from TEOS (red dot) and sodium silicate (black square) (C inset); XRD spectra of silica derived from TEOS (red), and from sodium silicate (black) (D).

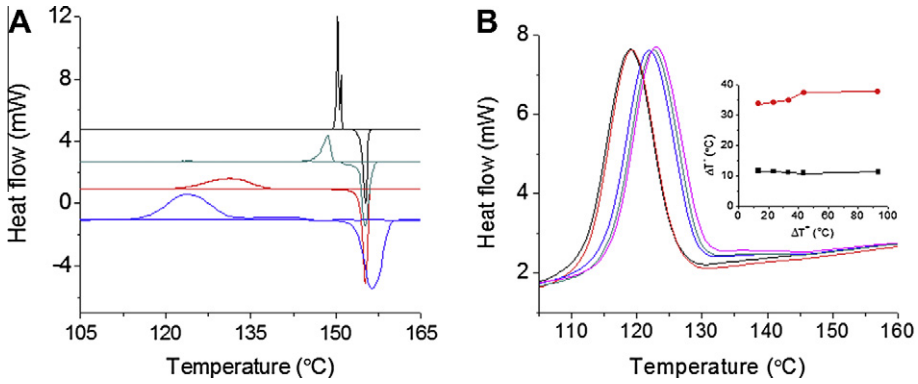

Figure 3. DSC curves of bulk indium (black), raw indium powders (red), indium nanoparticles in silica derived from TEOS (blue), and from sodium silicate (green) (A); DSC curves of indium nanoparticles in silica derived from TEOS at different over-heating (B); over-heating dependent super-cooling for indium nanoparticles in silica derived from TEOS (red dot), and from sodium silicate (black square) (B inset).

Table 1
Interfacial energy between indium and silica surfaces.

Indium		Cristobalite			Quartz				
		{100}	{1 1 1}	{1 1 0}	{1 0 1}	{1 1 1}	{1 0 0}	{1 1 0}	{0 0 1}
γ_{AB} (J/m2)	{0 0 1}	0.99928	0.63004	0.90591	0.94303	1.23057	1.13304	1.27002	1.29976
	{1 1 0}	0.90227	0.55352	0.81366	0.84886	1.12265	1.02958	1.16034	1.18877
	{1 0 0}	0.86508	0.52448	0.77836	0.8128	1.08112	0.98983	1.11811	1.14602
θ (°)	{0 0 1}	180	107	149	159	180	180	180	180
	{1 1 0}	128	89	117	121	180	147	180	180
	{1 0 0}	117	83	108	112	145	132	152	159
$\Delta G*$ (10–15 J)	{0 0 1}	9.2	6.5	9.1	9.2	9.2	78.9	19.8	58.9
	{1 1 0}	12.5	6.8	11.3	11.8	13.9	57.06	13.4	42.6
	{1 0 0}	13.5	6.8	11.9	12.6	16.1	47.5	11.3	37.2

cristobalite are smaller than those of indium-quartz. The contact angles and critical free energies of molten indium on different crystal faces of silica have been derived and shown in Table 1 [12,13]. In the case of TEOS-derived silica that is treated as a mixture of quartz with random orientation of crystal faces, molten indium does not wet and nucleation is homogeneous. In the case of silica derived from sodium silicate, molten indium has shown smaller contact angle, and energy barrier for nucleation is reduced, so as to reduce the super-cooling effect.

Super-cooling is related to thermal history of sample such as over-heating during melting process. In order to study effect of over-heating, thermal scans are carried out on indium nanoparticles coated inside silica derived from TEOS and sodium silicate. Figure 3B are DSC curves collected when silica encapsulated indium nanoparticles derived from TEOS are heated at 20 °C/min to the highest temperature and cooled down, where the highest temperatures are 170, 180, 190, 200 and 250 °C with over-heating of 14, 24, 34, 44 and 94 °C, respectively; the relation between super-cooling and over-heating for both nanoparticles silica encapsulated indium nanoparticles derived from TEOS and sodium silicate are shown in Figure 3B inset. In the case of TEOS-derived silica, super-cooling increases from 33.7 to 37.4 °C when over-heating increases from 14 to 44 °C, and remain the same when over-heating increases to 94 °C (red dot). In the case of sodium silicate derive silica, the over-heating has no affection to the super-cooling (black square). The degree of super-cooling (ΔT^{-}) depends on that of over-heating (ΔT^{+}) as $\Delta T^{-}/\Delta T^{+} = tg\theta$, where θ is contact angle of molten nanoparticle on silica. This is due to existence of small crystals over melting temperature which reduces super-cooling of molten nanoparticles by facilitating nucleation. If nanoparticles are overheated to a large extent, the number of crystals decreases significantly, and homogeneous nucleation occurs during freezing due to lack of nucleating sites. From super-cooling-overheating relations, the contact angles of molten indium nanoparticles on TEOS-derived silica and sodium silicate derived silica are determined to be 6.8° and 0°, respectively. These values are much smaller than those (i.e., 145° and 83° on In(1 0 0) and SiO_2 (1 1 1) interfaces) derived from Table 1, though the trends are the same (i.e., indium on sodium silicate derived silica has smaller contact angle). One possible reason for the large difference is that the data shown in Table 1 are derived from molten metal drops on single crystal surfaces, while those of nanoparticles are measured from nanoparticles with surrounding shells. The second possibility is that capillary interaction induced by stacking of small crystals (roughness) might have large effect on solidification.

The heating and cooling rates affect super-cooling of nanoparticles. In one experiment, encapsulated indium nanoparticles are heated to 165 °C (10 °C over-heating) at rate of 20 °C/min, and cooled at various rates; in another set, nanoparticles are heated at various rate and cool down at 20 °C/min. Super-cooling of nanoparticles in TEOS-derived silica at 1, 5, 10, 20, and 40 °C/min are 32, 33, 34, 36, and 41 °C (Figure 4A), respectively; those of nanoparticles in sodium silicate derived silica at 1, 5, 10, 20, and 40 °C/min are 3.9, 6.1, 8.3, 10.2, and 14 °C (not shown). The heating (cooling) rate dependent super-cooling is shown in Figure 4B, where slopes of super-cooling versus heating (cooling) rate for both types of nanoparticles are almost linear, meaning thermal inertia of measurement chamber is a common origin, and the effective thermal inertia of chamber is determined to be 0.22 J/°C.

The degree of super-cooling (ΔT) is normally defined as temperature difference between melting peak and cooling peak, but, when heat transfer efficiency in a loop is concerned, the degree of super-cooling should be the difference between terminal temperatures of melting and cooling curves, where peak widths should be taken into considered. In DSC curve, peak width depends on heat transfer from heater to sample, thermal conductivity of atmosphere, and temper-

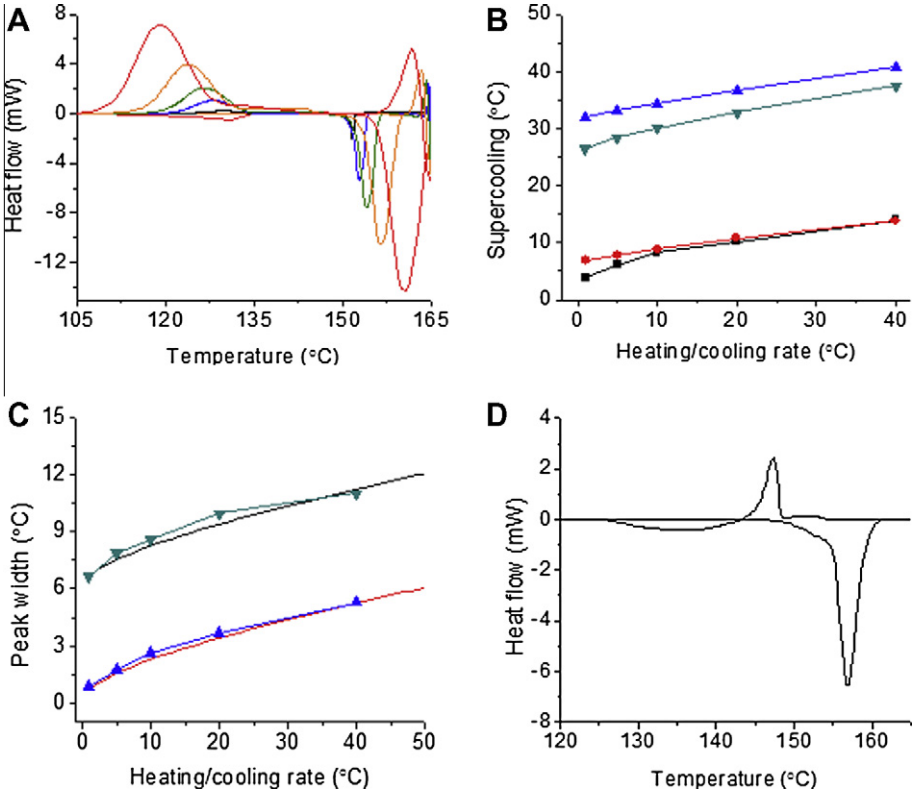

Figure 4. DSC curves of super-cooling as functions of indium nanoparticles in TEOS-derived silica at different cooling and heating rates (black, blue, green, orange, and red are at heating and cooling speed of 1, 5, 10, 20, and 40 °C/min, respectively (A); super-cooling as functions of heating and cooling rates for nanoparticles inside silica derived from TEOS (up triangle for heating and down triangle for cooling), and from sodium silicate (square for heating, and circle for cooling) (B); half peak widths as function of heating (up triangle) or cooling (down triangle) rates where solid lines are simulated results (C); DSC curve of indium nanoparticles coated in silica derived from sodium silicate after 100 times heating–cooling cycles in PAO (D).

ature ramp rate, and can be described by Gray's model based on energy conservation and Newton's law. The melting peak shape for a small amount of sample consists of two half-peaks, where the first has straight line slope and the second shows an exponential decay [14]. The width of melting peak can be derived as

$$w = \frac{1}{2}\beta \cdot \Delta t = \frac{1}{2}\beta \cdot (t_1 + t_2) = \frac{1}{2}\beta RC_5\left[\left(\sqrt{1+\frac{2\Delta H}{RC_s^2\beta}}-1\right)+ln(100)\right] \quad (3)$$

where R is thermal resistance (0.3 °C/mW), β is heating rate, Δt is melting time, t_1 and t_2 are rising and decaying times, respectively, ΔH and C_s are the energy required to melt material and the sample heat capacity, respectively. t_2 is defined as the time for heat flow fall below 1% of its maximum value. For 10 mg of silica encapsulated indium nanoparticles with 100 nm radius of indium core and 50 nm thickness of silica shell, ΔH and C_s are 166.2 mJ and 4.3 mJ/°C by taking densities of indium and silica as 7.3 and 2.2 g/cm^{-3}, respectively. Figure 4C shows heating rate dependent peak width of silica encapsulated indium nanoparticles after replacing all symbols with numbers, where peaks are wider when heating rates increase, nanoparticles in silica derived from TEOS and sodium silicate show similar trend, and the lines are simulated results according to Eq. (3). On the other hand, the cooling rate affects width of solidifying peak. Indium nanoparticles inside silica derived from TEOS and sodium silicate are heated to 165 °C (10 °C over-heating) and cooled down to 50 °C at various rates. Figure 4C also shows solidifying peaks are wider at higher cooling rates, and the dependence of peak width on cooling rate follows the similar rule as that of heating peaks. In addition, the widths of solidifying peaks are larger compared to melting peaks at the same heating/cooling rate, which is probably due to difference in thermal resistance at different temperatures, but peak areas at the same heating and cooling rates are the same, which means constant thermal mass of nanoparticles, and good encapsulation of silica shell.

At last, indium nanoparticles with silica shells derived from sodium silicate are dispersed in poly-α-olefin (PAO) to test their heat transfer ability. Figure 4D shows a DSC curve measured at ramp rate of 20 °C/min, and cooling rate of 20 °C/min, where the heating–cooling cycles have been repeated between 150 and 165 °C for 100 times. The repeatable DSC curves indicate that silica derived from sodium silicate is sufficiently strong to prevent molten nanoparticles from leakage or agglomeration despite their porous structures. The effective specific heat of indium nanoparticles in sodium silicate derived silica shell is 6.8 J/gK by considering super-cooling and peak width; in comparison, the effective specific heat of indium nanoparticles encapsulated in TEOS-derived silica (3.5 J/gK), and the specific heat of PAO (2.7 J/gK) are much smaller.

In summary, super-cooling of indium nanoparticles can be reduced by heterogeneous nucleation on silica derived from sodium silicate. Both surface roughness and crystal structure of silica can lower the threshold of nucleation, and degree of super-cooling. The effects of over-heating, heating and cooling rates can be understood from heterogeneous nucleation and thermal inertia of analysis instrument. By reducing super-cooling of indium nanoparticles, heat transfer with nanoparticle suspension can be enhanced.

Acknowledgment

This project has been supported by Air Force Research Laboratory (AFRL) and National Science Foundation (No. NSF-CBET-0828466).

References

[1] Y. Hong et al., ACS Appl. Mater. Interface 2 (2010) 1685.
[2] Z.H. Han, F.Y. Cao, B. Yang, Appl. Phys. Lett. 92 (2008) 243104.
[3] J.L. Alvarado, C. Marsh, C. Sohn, M. Vilceus, V. Hock, G. Phetteplace, T. Newell, J. Therm. Anal. Calorim. 86 (2006) 505.
[4] M. Faucheux, G. Muller, M. Havet, A. LeBail, Int. J. Refrig. 29 (2006) 1218.
[5] Y.F. Fan, X.X. Zhang, X.C. Wang, J. Li, Q.B. Zhu, Thermochim. Acta 413 (2004) 1.
[6] X.X. Zhang, Y.F. Fan, X.M. Tao, K.L. Yick, J. Colloid Interface Sci. 281 (2005) 299.
[7] A.F. Heneghan, A.D.J. Haymet, Chem. Phys. Lett. 368 (2003) 177.
[8] S. Ogawa, M. Koga, S. Osanai, Chem. Phys. Lett. 480 (2009) 86.
[9] H.Y. Tong, F.G. Shi, Appl. Phys. Lett. 70 (1996) 841.
[10] D. Turnbull, J. Chem. Phys. 18 (1950) 198.
[11] J.T. Zhang, Y.N. Wang, Int. J. Thermophys. 29 (2008) 844.
[12] V.V. Murashov, E. Demchuk, Surf. Sci. 595 (2005) 6.
[13] L. Vitos, A.V. Ruban, H.L. Skriver, J. Kollár, Surf. Sci. 411 (1998) 186.
[14] G. Wang, I.R. Harrison, Thermochim. Acta 231 (1994) 203.